Chapter 5

Cocontinuous morphologies in polymer blends (3D simulation)

Polymer-polymer blends offer an important route to materials with unique combinations of properties not available in a single polymer [127]. Such materials can be produced via intense mixing of immiscible polymer blends and subsequent cooling below the melt temperature of one of the components [88] to produce a solid. During mixing, a variety of non-equilibrium heterogeneous microstructures (morphologies) can form which can then be trapped during the cooling process. Possible non-equilibrium microstructures include droplet/matrix, fibers, lamella, and cocontinuous, sponge-like structures in which each component phase is continuous. Sample SEM images of blends with cocontinuous and droplet morphologies are presented in Fig. 5.1, which shows SEM images of PEO/PS blends; a 50/50 blend with PEO removed by water extraction (left) and a 90/10 blend with PS removed by toluene extraction (right). This image is taken from [66].

Cocontinuous microstructures are distinguished by having interpenetrating, and self-supporting continuous phases in three dimensions. The resulting fluid is sponge-like. A precise mathematical definition is posed in section 5.4 that is suitable for our 3D numerical simulations and comparison with experiments. Let us illustrate the droplet/matrix and cocontinuous morphologies by a cartoon. Fig. 5.2 shows 12% volume fraction droplet/matrix phase before extraction of matrix phase and Fig. 5.3 shows after extraction of the matrix phase, it is not self-supportive. But, interface is shown in Fig. 5.4, which is 50% volume fraction cocontinuous phase remains a self-supportive morphology in Fig. 5.5 even after extraction of the other phase.

Blends with cocontinuous morphology have several applications including conductive packaging for

static dissipation, materials with improved mechanical properties, and barrier film structures. Although cocontinuous polymer blends have found numerous applications, their formation is not well understood. In addition, cocontinuity in polymer-polymer blends is difficult to confirm experimentally. The goals of this research include the development of numerical methods capable of simulating the coalescence cascade to form co-cocontinuous structures, the investigation of optimal processing conditions and testing detection techniques[1].

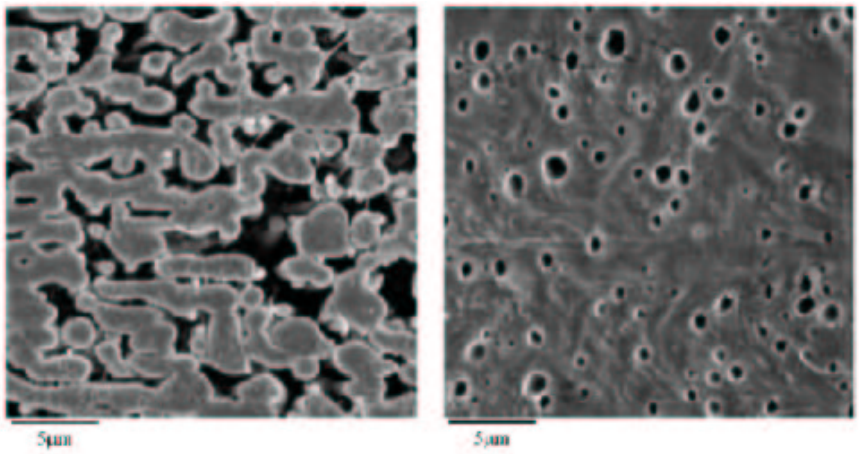

Figure 5.1: SEM images of PEO/PS blends; a 50/50 blend with PEO removed by water extraction (left) and a 90/10 blend with PS removed by toluene extraction (right) [66].

Intuitively, the amount of interface per unit area increases as the amount of minor component increases and then decreases when the morphology becomes cocontinuous as elongated structures become connected to reduce the interfacial area. This is confirmed in preliminary experiments [66].

Finally, current experimental detection techniques are indirect and involve the measurements of conductivity and of surface area, for example. In a simulation, however, we can directly determine whether a cocontinuous structure is present.

5.1 Governing equations

Cocontinuous morphology is a fully three dimensional phenomenon, therefore it is necessary to simulate the evolution in three dimensions. In the numerical experiments presented here, we approximate

[1] Project joint with John Lowengrub and Chris Macosko (Chem. Eng., U. Minn), Vittoro Cristini and Jeff Galloway.

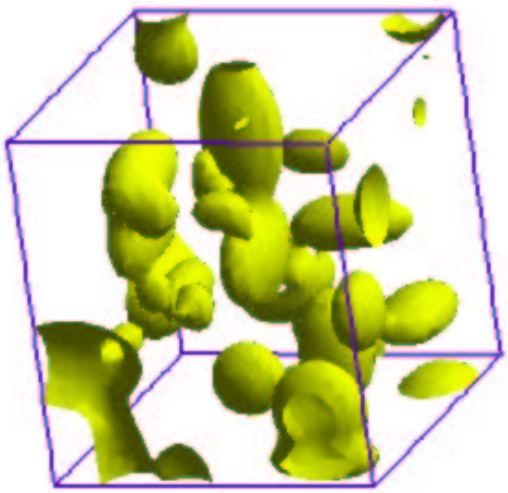

Figure 5.2: Before extraction (12%).

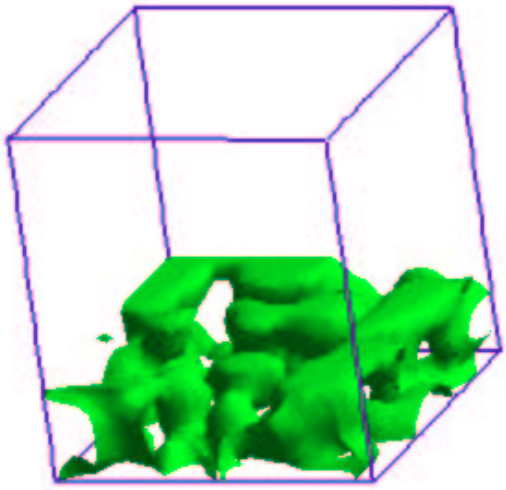

Figure 5.3: After extraction (12%).

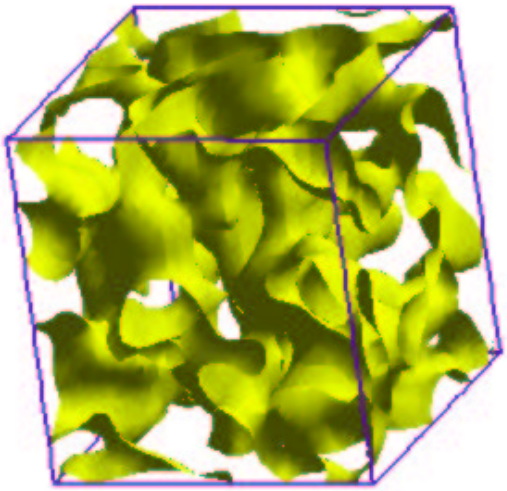

Figure 5.4: Before extraction (50%).

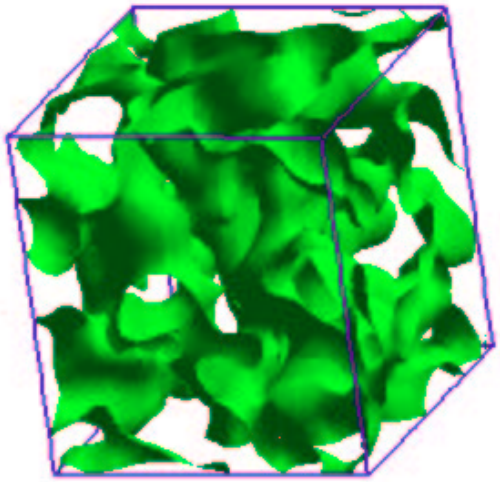

Figure 5.5: After extraction (50%).

polymers by Newtonian viscous fluids, so the governing equations are

$$\mathbf{u}_t + \mathbf{u}\cdot\nabla\mathbf{u} = -\nabla p + \frac{1}{\mathbf{Re}}\nabla\cdot[\eta(c)(\nabla\mathbf{u}+\nabla\mathbf{u}^T)] - \frac{\epsilon}{\mathbf{We}}(\Delta c\nabla c - \frac{1}{2}\nabla|\nabla c|^2), \quad (5.1.1)$$

$$\nabla\cdot\mathbf{u} = 0, \quad (5.1.2)$$

$$\frac{\partial c}{\partial t} + \nabla\cdot(c\mathbf{u}) = \frac{1}{\mathbf{Pe}}\nabla\cdot(M(c)\nabla\mu), \quad (5.1.3)$$

$$\mu = \frac{dF(c)}{dc} - \epsilon^2\Delta c, \quad (5.1.4)$$

where

$$M(c) = c(1-c), \;\; F(c) = \frac{1}{4}c^2(1-c)^2.$$

The non-dimensional numbers (**Re**, **We**, and **Pe**) were defined at the chapter 4.

5.2 3 Dimensional Discretization of Cahn-Hilliard equation

Let $s = -\nabla\cdot(c\mathbf{u})$, then the discretization of Eq. (5.1.3) is

$$\frac{c_{ijk}^{n+1} - c_{ijk}^n}{\Delta t} = \frac{1}{\mathbf{Pe}}\nabla\cdot[M(c_{ijk}^{n+\frac{1}{2}})\nabla\mu_{ijk}^{n+\frac{1}{2}}] + s_{ijk}^{n+\frac{1}{2}}.$$

$$\begin{aligned}
\frac{c_{ijk}^{n+1}}{\Delta t} &- \frac{M(c_{i+\frac{1}{2},jk}^{n+\frac{1}{2}})(\mu_{i+1,jk}^{n+\frac{1}{2}} - \mu_{ijk}^{n+\frac{1}{2}}) - M(c_{i-\frac{1}{2},jk}^{n+\frac{1}{2}})(\mu_{ijk}^{n+\frac{1}{2}} - \mu_{i-1,jk}^{n+\frac{1}{2}})}{\mathbf{Pe}\Delta x^2} \\
&- \frac{M(c_{i,j+\frac{1}{2},k}^{n+\frac{1}{2}})(\mu_{i,j+1,k}^{n+\frac{1}{2}} - \mu_{ijk}^{n+\frac{1}{2}}) - M(c_{i,j-\frac{1}{2},k}^{n+\frac{1}{2}})(\mu_{ijk}^{n+\frac{1}{2}} - \mu_{i,j-1,k}^{n+\frac{1}{2}})}{\mathbf{Pe}\Delta y^2} \\
&- \frac{M(c_{ij,k+\frac{1}{2}}^{n+\frac{1}{2}})(\mu_{ij,k+1}^{n+\frac{1}{2}} - \mu_{ijk}^{n+\frac{1}{2}}) - M(c_{ij,k-\frac{1}{2}}^{n+\frac{1}{2}})(\mu_{ijk}^{n+\frac{1}{2}} - \mu_{ij,k-1}^{n+\frac{1}{2}})}{\mathbf{Pe}\Delta z^2} \\
&= \frac{c_{ijk}^n}{\Delta t} + s_{ijk}^{n+\frac{1}{2}}
\end{aligned}$$

$$\begin{aligned}
\frac{c_{ijk}^{n+1}}{\Delta t} &+ \left[\frac{M(c_{i+\frac{1}{2},jk}^{n+\frac{1}{2}})+M(c_{i-\frac{1}{2},jk}^{n+\frac{1}{2}})}{\mathbf{Pe}\Delta x^2}+\frac{M(c_{i,j+\frac{1}{2},k}^{n+\frac{1}{2}})+M(c_{i,j-\frac{1}{2},k}^{n+\frac{1}{2}})}{\mathbf{Pe}\Delta y^2}\right. \\
&\left.+\frac{M(c_{ij,k+\frac{1}{2}}^{n+\frac{1}{2}})+M(c_{ij,k-\frac{1}{2}}^{n+\frac{1}{2}})}{\mathbf{Pe}\Delta z^2}\right]\mu_{ijk}^{n+\frac{1}{2}} \\
&= \frac{M(c_{i+\frac{1}{2},jk}^{n+\frac{1}{2}})\mu_{i+1,jk}^{n+\frac{1}{2}}+M(c_{i-\frac{1}{2},jk}^{n+\frac{1}{2}})\mu_{i-1,jk}^{n+\frac{1}{2}}}{\mathbf{Pe}\Delta x^2} \\
&+ \frac{M(c_{i,j+\frac{1}{2},k}^{n+\frac{1}{2}})\mu_{i,j+1,k}^{n+\frac{1}{2}}+M(c_{i,j-\frac{1}{2},k}^{n+\frac{1}{2}})\mu_{i,j-1,k}^{n+\frac{1}{2}}}{\mathbf{Pe}\Delta y^2} \\
&+ \frac{M(c_{ij,k+\frac{1}{2}}^{n+\frac{1}{2}})\mu_{ij,k+1}^{n+\frac{1}{2}}+M(c_{ij,k-\frac{1}{2}}^{n+\frac{1}{2}})\mu_{ij,k-1}^{n+\frac{1}{2}}}{\mathbf{Pe}\Delta z^2}+\frac{c_{ijk}^{n}}{\Delta t}+s_{ijk}^{n+\frac{1}{2}}
\end{aligned} \tag{5.2.5}$$

And the discretization of Eq. (5.1.4) is

$$\mu_{ijk}^{n+\frac{1}{2}}=\frac{1}{2}(f(c_{ijk}^{n+1})+f(c_{ijk}^{n}))-\frac{\epsilon^2}{2}(\Delta c_{ijk}^{n+1}+\Delta c_{ijk}^{n}).$$

$$\begin{aligned}
-[\frac{\epsilon^2}{\Delta x^2}+\frac{\epsilon^2}{\Delta y^2}+\frac{\epsilon^2}{\Delta z^2}]c_{ijk}^{n+1}+\mu_{ijk}^{n+\frac{1}{2}} &= \frac{1}{2}f(c_{ijk}^{n+1})+\frac{1}{2}f(c_{ijk}^{n})-\frac{\epsilon^2}{2}\Delta c_{ijk}^{n}-\frac{\epsilon^2}{2\Delta x^2}(c_{i+1,jk}^{n+1}+c_{i-1,jk}^{n+1}) \\
&\quad -\frac{\epsilon^2}{2\Delta y^2}(c_{i,j+1,k}^{n+1}+c_{i,j-1,k}^{n+1})-\frac{\epsilon^2}{2\Delta z^2}(c_{ij,k+1}^{n+1}+c_{ij,k-1}^{n+1}).
\end{aligned}$$

Linearize $f(c_{ijk}^{n+1})$ about c_{ijk}^{m} to get

$$f(c_{ijk}^{n+1})=f(c_{ijk}^{m})+\frac{df}{dc}(c_{ijk}^{m})(c_{ijk}^{n+1}-c_{ijk}^{m}).$$

Then

$$\begin{aligned}
-\left[\frac{\epsilon^2}{\Delta x^2}+\frac{\epsilon^2}{\Delta y^2}+\frac{\epsilon^2}{\Delta z^2}+\frac{1}{2}\frac{df}{dc}(c_{ijk}^{m})\right]c_{ijk}^{n+1}+\mu_{ijk}^{n+1} &= \frac{1}{2}f(c_{ijk}^{n})-\frac{\epsilon^2}{2}\Delta c_{ijk}^{n}+\frac{1}{2}f(c_{ijk}^{m}) \\
-\frac{1}{2}\frac{df}{dc}(c_{ijk}^{m})c_{ijk}^{m} &- \frac{\epsilon^2}{2\Delta x^2}(c_{i+1,jk}^{n+1}+c_{i-1,jk}^{n+1}) \\
-\frac{\epsilon^2}{2\Delta y^2}(c_{i,j+1,k}^{n+1}+c_{i,j-1,k}^{n+1}) &- \frac{\epsilon^2}{2\Delta z^2}(c_{ij,k+1}^{n+1}+c_{ij,k-1}^{n+1}).
\end{aligned} \tag{5.2.6}$$

We use discrete Eqs. (5.2.5) and (5.2.6) in the relaxation step in a multigrid solver which we described in chapter 2.

5.3 3D discretization of Navier-Stokes equations

Let $\mathbf{F} = -\frac{\epsilon}{\mathbf{We}}(\Delta c \nabla c - \frac{1}{2}\nabla|\nabla c|^2)$, then the discretizations of Eqs. (5.1.1) and (5.1.2) are

$$\begin{aligned}\frac{\mathbf{u}^{n+1}-\mathbf{u}^n}{\Delta t} + [\mathbf{u}\cdot\nabla\mathbf{u}]^{n+\frac{1}{2}} &= -\nabla p^{n+\frac{1}{2}} + \frac{1}{2\mathbf{Re}}\nabla\cdot[\eta^n(\nabla\mathbf{u}^n + (\nabla\mathbf{u}^n)^T)] \\ &\quad + \frac{1}{2\mathbf{Re}}\nabla\cdot[\eta^{n+1}(\nabla\mathbf{u}^{n+1} + (\nabla\mathbf{u}^{n+1})^T)] + \mathbf{F}^{n+\frac{1}{2}}, \\ \nabla\cdot\mathbf{u}^{n+1} &= 0.\end{aligned}$$

We use the projection method [6]. In projection method, the procedure is given by

Step 1: Solve for the intermediate velocity field $\mathbf{u}^*$

$$\begin{aligned}\frac{\mathbf{u}^*-\mathbf{u}^n}{\Delta t} + [\mathbf{u}\cdot\nabla\mathbf{u}]^{n+\frac{1}{2}} &= -\nabla p^{n-\frac{1}{2}} + \frac{1}{2\mathbf{Re}}\nabla\cdot[\eta^n(\nabla\mathbf{u}^n + (\nabla\mathbf{u}^n)^T)] \\ &\quad + \frac{1}{2\mathbf{Re}}\nabla\cdot[\eta^{n+1}(\nabla\mathbf{u}^* + (\nabla\mathbf{u}^*)^T)] + \mathbf{F}^{n+\frac{1}{2}}.\end{aligned} \tag{5.3.7}$$

Step 2: Perform the projection

$$\begin{aligned}\mathbf{u}^* &= \mathbf{u}^{n+1} + \Delta t\nabla\phi, \\ \Delta\phi &= \nabla\cdot\left(\frac{\mathbf{u}^*-\mathbf{u}^n}{\Delta t}\right).\end{aligned}$$

Step 3: Update the pressure

$$p^{n+\frac{1}{2}} = p^{n-\frac{1}{2}} + \phi.$$

Now, we describe this procedure in more detail. Let's rewrite Eq. (5.3.7)

$$\begin{aligned}\mathbf{u}^* - \frac{\Delta t}{2\mathbf{Re}}\nabla\cdot[\eta^{n+1}(\nabla\mathbf{u}^* + (\nabla\mathbf{u}^*)^T)] &= \mathbf{u}^n - \Delta t[\mathbf{u}\cdot\nabla\mathbf{u}]^{n+\frac{1}{2}} - \Delta t\nabla p^{n-\frac{1}{2}} \\ &\quad + \frac{\Delta t}{2\mathbf{Re}}\nabla\cdot[\eta^n(\nabla\mathbf{u}^n + (\nabla\mathbf{u}^*)^T)] + \Delta t\mathbf{F}^{n+\frac{1}{2}}.\end{aligned} \tag{5.3.8}$$

Let right hand side of equation (5.3.8) be S^n.

$$\mathbf{u}^* - \frac{\Delta t}{2\mathbf{Re}}\nabla\cdot[\eta^{n+1}(\nabla\mathbf{u}^* + (\nabla\mathbf{u}^*)^T)] = S^n = ({s_1}^n, {s_2}^n, {s_3}^n),$$

Then by using a Gauss-Seidel iteration, the relaxation scheme (smoother) becomes as follows :

$$
\begin{aligned}
[1 \;+\; & \frac{\Delta t}{2h^2\mathbf{Re}}(2\eta_{i+\frac{1}{2},jk} + 2\eta_{i-\frac{1}{2},jk} + \eta_{i,j+\frac{1}{2},k} + \eta_{i,j-\frac{1}{2},k} + \eta_{ij,k+\frac{1}{2}} + \eta_{ij,k-\frac{1}{2}})]u^*_{i,j} \\
= \;& {s_1}^n + \frac{\Delta t}{2h^2\mathbf{Re}}[2\eta_{i+\frac{1}{2},jk}u^*_{i+1,jk} + 2\eta_{i-\frac{1}{2},jk}u^*_{i-1,jk} + \eta_{i,j+\frac{1}{2},k}u^*_{i,j+1,k} \\
& + \eta_{i,j-\frac{1}{2},k}u^*_{i,j-1,k} + \eta_{ij,k+\frac{1}{2}}u^*_{ij,k+1} + \eta_{ij,k-\frac{1}{2}}u^*_{ij,k-1} \\
& + \frac{\eta_{i,j+\frac{1}{2},k}(v^*_{i+1,j+1,k} - v^*_{i-1,j+1,k} + v^*_{i+1,jk} - v^*_{i-1,jk})}{4} \\
& - \frac{\eta_{i,j-\frac{1}{2},k}(v^*_{i+1,jk} - v^*_{i-1,jk} + v^*_{i+1,j-1,k} - v^*_{i-1,j-1,k})}{4} \\
& + \frac{\eta_{ij,k+\frac{1}{2}}(w^*_{i+1,j,k+1} - w^*_{i-1,j,k+1} + w^*_{i+1,jk} - w^*_{i-1,jk})}{4} \\
& - \frac{\eta_{ij,k-\frac{1}{2}}(w^*_{i+1,jk} - w^*_{i-1,jk} + w^*_{i+1,j,k-1} - w^*_{i-1,j,k-1})}{4}],
\end{aligned}
$$

$$
\begin{aligned}
[1 \;+\; & \frac{\Delta t}{2h^2\mathbf{Re}}(\eta_{i+\frac{1}{2},jk} + \eta_{i-\frac{1}{2},jk} + 2\eta_{i,j+\frac{1}{2},k} + 2\eta_{i,j-\frac{1}{2},k} + \eta_{ij,k+\frac{1}{2}} + \eta_{ij,k-\frac{1}{2}})]v^*_{i,j} \\
= \;& {s_2}^n + \frac{\Delta t}{2h^2\mathbf{Re}}[\eta_{i+\frac{1}{2},jk}v^*_{i+1,jk} + \eta_{i-\frac{1}{2},jk}v^*_{i-1,jk} + 2\eta_{i,j+\frac{1}{2},k}v^*_{i,j+1,k} \\
& + 2\eta_{i,j-\frac{1}{2},k}v^*_{i,j-1,k} + \eta_{ij,k+\frac{1}{2}}v^*_{ij,k+1} + \eta_{ij,k-\frac{1}{2}}v^*_{ij,k-1} \\
& + \frac{\eta_{i+\frac{1}{2},jk}(u^*_{i+1,j+1,k} - u^*_{i+1,j-1,k} + u^*_{i,j+1,k} - u^*_{i,j-1,k})}{4} \\
& - \frac{\eta_{i-\frac{1}{2},jk}(u^*_{i,j+1,k} - u^*_{i,j-1,k} + u^*_{i-1,j+1,k} - u^*_{i-1,j-1,k})}{4} \\
& + \frac{\eta_{ij,k+\frac{1}{2}}(w^*_{i,j+1,k+1} - w^*_{i,j-1,k+1} + w^*_{i,j+1,k} - w^*_{i,j-1,k})}{4} \\
& - \frac{\eta_{ij,k-\frac{1}{2}}(w^*_{i,j+1,k} - w^*_{i,j-1,k} + w^*_{i,j+1,k-1} - w^*_{i,j-1,k-1})}{4}],
\end{aligned}
$$

$$
\begin{aligned}
[1 \quad + \quad & \frac{\Delta t}{2h^2\mathbf{Re}}(\eta_{i+\frac{1}{2},jk}+\eta_{i-\frac{1}{2},jk}+\eta_{i,j+\frac{1}{2},k}+\eta_{i,j-\frac{1}{2},k}+2\eta_{ij,k+\frac{1}{2}}+2\eta_{ij,k-\frac{1}{2}})]w^*_{i,j} \\
= \quad & {s_3}^n + \frac{\Delta t}{2h^2\mathbf{Re}}[\eta_{i+\frac{1}{2},jk}w^*_{i+1,jk}+\eta_{i-\frac{1}{2},jk}w^*_{i-1,jk}+\eta_{i,j+\frac{1}{2},k}w^*_{i,j+1,k} \\
& + \eta_{i,j-\frac{1}{2},k}w^*_{i,j-1,k}+2\eta_{ij,k+\frac{1}{2}}w^*_{ij,k+1}+2\eta_{ij,k-\frac{1}{2}}w^*_{ij,k-1} \\
& + \frac{\eta_{i+\frac{1}{2},jk}(u^*_{i+1,j,k+1}-u^*_{i+1,j,k-1}+u^*_{ij,k+1}-u^*_{ij,k-1})}{4} \\
& - \frac{\eta_{i-\frac{1}{2},jk}(u^*_{ij,k+1}-u^*_{ij,k-1}+u^*_{i-1,j,k+1}-u^*_{i-1,j,k-1})}{4} \\
& + \frac{\eta_{i,j+\frac{1}{2},k}(v^*_{i,j+1,k+1}-v^*_{i,j+1,k-1}+v^*_{ij,k+1}-v^*_{ij,k-1})}{4} \\
& - \frac{\eta_{i,j-\frac{1}{2},k}(v^*_{ij,k+1}-v^*_{ij,k-1}+v^*_{i,j-1,k+1}-v^*_{i,j-1,k-1})}{4}].
\end{aligned}
$$

We suppressed the $n+1$ superscript time indices on the viscosity term η for clear expressions. We solve this $\mathbf{u}^*$ by using a linear multigrid method which we described in chapter 2 appendix 8.B.

The viscous terms $\nabla \cdot [\eta(\nabla \mathbf{u} + \nabla \mathbf{u}^T)]$ are discretized as follows:

$$
\begin{aligned}
\nabla \cdot [\eta(\nabla \mathbf{u} + \nabla \mathbf{u}^T)] &= \nabla \cdot \left[\eta \begin{pmatrix} 2u_x & u_y+v_x & u_z+w_x \\ v_x+u_y & 2v_y & v_z+w_y \\ w_x+u_z & w_y+v_z & 2w_z \end{pmatrix} \right] \\
&= \begin{bmatrix} 2(\eta u_x)_x+(\eta u_y)_y+(\eta v_x)_y+(\eta u_z)_z+(\eta w_x)_z \\ (\eta u_y)_x+(\eta v_x)_x+2(\eta v_y)_y+(\eta v_z)_z+(\eta w_y)_z \\ (\eta w_x)_x+(\eta u_z)_x+(\eta w_y)_y+(\eta v_z)_y+2(\eta w_z)_z \end{bmatrix}
\end{aligned}
$$

The first component of the viscous term $\nabla \cdot [\eta(c)(\nabla \mathbf{u} + \nabla \mathbf{u}^T)]$ is discretized as

$$(\mathcal{L})^1_{ijk} = \begin{pmatrix} \frac{2\eta_{i+\frac{1}{2},jk}(u_{i+1,jk}-u_{ijk})-2\eta_{i-\frac{1}{2},jk}(u_{ijk}-u_{i-1,jk})}{\Delta x^2} \\ +\frac{\eta_{i,j+\frac{1}{2},k}(u_{i,j+1,k}-u_{ijk})-\eta_{i,j-\frac{1}{2},k}(u_{ijk}-u_{i,j-1,k})}{\Delta y^2} \\ +\frac{\eta_{ij,k+\frac{1}{2}}(u_{ij,k+1}-u_{ijk})-\eta_{ij,k-\frac{1}{2}}(u_{ijk}-u_{ij,k-1})}{\Delta z^2} \\ +\frac{\eta_{i,j+\frac{1}{2},k}(v_{i+1,j+1,k}-v_{i-1,j+1,k}+v_{i+1,jk}-v_{i-1,jk})}{4\Delta x\Delta y} \\ -\frac{\eta_{i,j-\frac{1}{2},k}(v_{i+1,jk}-v_{i-1,jk}+v_{i+1,j-1,k}-v_{i-1,j-1,k})}{4\Delta x\Delta y} \\ +\frac{\eta_{ij,k+\frac{1}{2}}(w_{i+1,j,k+1}-w_{i-1,j,k+1}+w_{i+1,jk}-w_{i-1,jk})}{4\Delta x\Delta z} \\ -\frac{\eta_{ij,k-\frac{1}{2}}(w_{i+1,jk}-w_{i-1,jk}+w_{i+1,j,k-1}-w_{i-1,j,k-1})}{4\Delta x\Delta z} \end{pmatrix},$$

The second component of the viscous term $\nabla \cdot [\eta(c)(\nabla \mathbf{u} + \nabla \mathbf{u}^T)]$ is discretized as

$$(\mathcal{L})^2_{ijk} = \begin{pmatrix} \frac{\eta_{i+\frac{1}{2},jk}(v_{i+1,jk}-v_{ijk})-\eta_{i-\frac{1}{2},jk}(v_{ijk}-v_{i-1,jk})}{\Delta x^2} \\ +\frac{2\eta_{i,j+\frac{1}{2},k}(v_{i,j+1,k}-v_{ijk})-2\eta_{i,j-\frac{1}{2},k}(v_{ijk}-v_{i,j-1,k})}{\Delta y^2} \\ +\frac{\eta_{ij,k+\frac{1}{2}}(v_{ij,k+1}-v_{ijk})-\eta_{ij,k-\frac{1}{2}}(v_{ijk}-v_{ij,k-1})}{\Delta z^2} \\ +\frac{\eta_{i+\frac{1}{2},jk}(u_{i+1,j+1,k}-u_{i+1,j-1,k}+u_{i,j+1,k}-u_{i,j-1,k})}{4\Delta x\Delta y} \\ -\frac{\eta_{i-\frac{1}{2},jk}(u_{i,j+1,k}-u_{i,j-1,k}+u_{i-1,j+1,k}-u_{i-1,j-1,k})}{4\Delta x\Delta y} \\ +\frac{\eta_{ij,k+\frac{1}{2}}(w_{i,j+1,k+1}-w_{i,j-1,k+1}+w_{i,j+1,k}-w_{i,j-1,k})}{4\Delta y\Delta z} \\ -\frac{\eta_{ij,k-\frac{1}{2}}(w_{i,j+1,k}-w_{i,j-1,k}+w_{i,j+1,k-1}-w_{i,j-1,k-1})}{4\Delta y\Delta z} \end{pmatrix},$$

The third component of the viscous term $\nabla \cdot [\eta(c)(\nabla \mathbf{u} + \nabla \mathbf{u}^T)]$ is discretized as

$$(\mathcal{L})^3_{ijk} = \begin{pmatrix} \frac{\eta_{i+\frac{1}{2},jk}(w_{i+1,jk}-w_{ijk})-\eta_{i-\frac{1}{2},jk}(w_{ijk}-w_{i-1,jk})}{\Delta x^2} \\ +\frac{\eta_{i,j+\frac{1}{2},k}(w_{i,j+1,k}-w_{ijk})-\eta_{i,j-\frac{1}{2},k}(w_{ijk}-w_{i,j-1,k})}{\Delta y^2} \\ +\frac{2\eta_{ij,k+\frac{1}{2}}(w_{ij,k+1}-w_{ijk})-2\eta_{ij,k-\frac{1}{2}}(w_{ijk}-w_{ij,k-1})}{\Delta z^2} \\ +\frac{\eta_{i+\frac{1}{2},jk}(u_{i+1,j,k+1}-u_{i+1,j,k-1}+u_{ij,k+1}-u_{ij,k-1})}{4\Delta x\Delta z} \\ -\frac{\eta_{i-\frac{1}{2},jk}(u_{ij,k+1}-u_{ij,k-1}+u_{i-1,j,k+1}-u_{i-1,j,k-1})}{4\Delta x\Delta z} \\ +\frac{\eta_{i,j+\frac{1}{2},k}(v_{i,j+1,k+1}-v_{i,j+1,k-1}+v_{ij,k+1}-v_{ij,k-1})}{4\Delta y\Delta z} \\ -\frac{\eta_{i,j-\frac{1}{2},k}(v_{ij,k+1}-v_{ij,k-1}+v_{i,j-1,k+1}-v_{i,j-1,k-1})}{4\Delta y\Delta z} \end{pmatrix},$$

where

$$\begin{aligned} \eta_{i+\frac{1}{2},jk} &= \frac{1}{2}[\eta(c_{ijk})+\eta(c_{i+1,jk})], \\ \eta_{i,j+\frac{1}{2},k} &= \frac{1}{2}[\eta(c_{ijk})+\eta(c_{i,j+1,k})], \\ \eta_{ij,k+\frac{1}{2}} &= \frac{1}{2}[\eta(c_{ijk})+\eta(c_{ij,k+1})]. \end{aligned}$$

The nonlinear advection terms $[\mathbf{u}\cdot\nabla\mathbf{u}]^{n+\frac{1}{2}}$, are evaluated using an explicit predictor-corrector scheme and require only the available data at t^n.

Predictor. In the predictor we extrapolate the velocity and density to the cell edges at $t^{n+\frac{1}{2}}$ using a second-order Taylor series expansion.

For edge $(i+\frac{1}{2},j,k)$ this gives

$$\begin{aligned} \mathbf{u}^{n+\frac{1}{2},L}_{i+\frac{1}{2},jk} &= \mathbf{u}^n_{ijk}+\frac{\Delta x}{2}\mathbf{u}^n_{x,ijk}+\frac{\Delta t}{2}\mathbf{u}^n_{t,ijk} \\ c^{n+\frac{1}{2},L}_{i+\frac{1}{2},jk} &= c^n_{ijk}+\frac{\Delta x}{2}c^n_{x,ijk}+\frac{\Delta t}{2}c^n_{t,ijk} \end{aligned}$$

extrapolating from (ijk), and

$$\begin{aligned} \mathbf{u}^{n+\frac{1}{2},R}_{i+\frac{1}{2},jk} &= \mathbf{u}^n_{i+1,jk}-\frac{\Delta x}{2}\mathbf{u}^n_{x,i+1,jk}+\frac{\Delta t}{2}\mathbf{u}^n_{t,i+1,jk} \\ c^{n+\frac{1}{2},R}_{i+\frac{1}{2},jk} &= c^n_{i+1,jk}-\frac{\Delta x}{2}c^n_{x,i+1,jk}+\frac{\Delta t}{2}c^n_{t,i+1,jk} \end{aligned}$$

extrapolating from $(i+1, j, k)$.

For edge $(i, j+\frac{1}{2}, k)$ this gives

$$\mathbf{u}^{n+\frac{1}{2},B}_{i,j+\frac{1}{2},k} = \mathbf{u}^n_{ijk} + \frac{\Delta y}{2}\mathbf{u}^n_{y,ijk} + \frac{\Delta t}{2}\mathbf{u}^n_{t,ijk}$$
$$c^{n+\frac{1}{2},B}_{i,j+\frac{1}{2},k} = c^n_{ijk} + \frac{\Delta y}{2}c^n_{y,ijk} + \frac{\Delta t}{2}c^n_{t,ijk}$$

extrapolating from (ijk), and

$$\mathbf{u}^{n+\frac{1}{2},F}_{i,j+\frac{1}{2},k} = \mathbf{u}^n_{i,j+1,k} - \frac{\Delta y}{2}\mathbf{u}^n_{y,i,j+1,k} + \frac{\Delta t}{2}\mathbf{u}^n_{t,i,j+1,k}$$
$$c^{n+\frac{1}{2},F}_{i,j+\frac{1}{2},k} = c^n_{i,j+1,k} - \frac{\Delta y}{2}c^n_{y,i,j+1,k} + \frac{\Delta t}{2}c^n_{t,i,j+1,k}$$

extrapolating from $(i, j+1, k)$.

For edge $(ij, k+\frac{1}{2})$ this gives

$$\mathbf{u}^{n+\frac{1}{2},D}_{ij,k+\frac{1}{2}} = \mathbf{u}^n_{ijk} + \frac{\Delta z}{2}\mathbf{u}^n_{z,ijk} + \frac{\Delta t}{2}\mathbf{u}^n_{t,ijk}$$
$$c^{n+\frac{1}{2},D}_{ij,k+\frac{1}{2}} = c^n_{ijk} + \frac{\Delta z}{2}c^n_{z,ijk} + \frac{\Delta t}{2}c^n_{t,ijk}$$

extrapolating from (ijk), and

$$\mathbf{u}^{n+\frac{1}{2},U}_{ij,k+\frac{1}{2}} = \mathbf{u}^n_{ij,k+1} - \frac{\Delta z}{2}\mathbf{u}^n_{z,ij,k+1} + \frac{\Delta t}{2}\mathbf{u}^n_{t,ij,k+1}$$
$$c^{n+\frac{1}{2},U}_{ij,k+\frac{1}{2}} = c^n_{ij,k+1} - \frac{\Delta z}{2}c^n_{z,ij,k+1} + \frac{\Delta t}{2}c^n_{t,ij,k+1}$$

extrapolating from $(ij, k+1)$.

The differential equation (5.1.3) is then used to eliminate the time derivatives to obtain

$$\begin{aligned}\mathbf{u}^{n+\frac{1}{2},L}_{i+\frac{1}{2},jk} &= \mathbf{u}^n_{ijk} + (\frac{\Delta x}{2} - \frac{u^n_{ijk}\Delta t}{2})\mathbf{u}^n_{x,ijk} - \frac{\Delta t}{2}(\widehat{v\mathbf{u}_y})_{ijk} - \frac{\Delta t}{2}(\widehat{w\mathbf{u}_z})_{ijk} \\ &\quad + \frac{\Delta t}{2}(\frac{1}{\mathbf{Re}}\nabla\cdot[\eta(\nabla\mathbf{u}^n_{ijk} + \nabla\mathbf{u}^{n\ T}_{ijk})] - \nabla p^{n-\frac{1}{2}}_{ijk} + F^n_{ijk}), \end{aligned} \tag{5.3.9}$$

$$\begin{aligned}\mathbf{u}^{n+\frac{1}{2},R}_{i+\frac{1}{2},jk} &= \mathbf{u}^n_{i+1,jk} - (\frac{\Delta x}{2} + \frac{u^n_{i+1,jk}\Delta t}{2})\mathbf{u}^n_{x,i+1,jk} - \frac{\Delta t}{2}(\widehat{v\mathbf{u}_y})_{i+1,jk} - \frac{\Delta t}{2}(\widehat{w\mathbf{u}_z})_{i+1,jk} \\ &\quad + \frac{\Delta t}{2}(\frac{1}{\mathbf{Re}}\nabla\cdot[\eta(\nabla\mathbf{u}^n_{i+1,jk} + \nabla\mathbf{u}^{n\ T}_{i+1,jk})] - \nabla p^{n-\frac{1}{2}}_{i+1,jk} + F^n_{i+1,jk}), \end{aligned} \tag{5.3.10}$$

$$\begin{aligned}\mathbf{u}^{n+\frac{1}{2},B}_{i,j+\frac{1}{2},k} &= \mathbf{u}^n_{ijk} + (\frac{\Delta y}{2} - \frac{v^n_{ijk}\Delta t}{2})\mathbf{u}^n_{y,ijk} - \frac{\Delta t}{2}(\widehat{u\mathbf{u}_x})_{ijk} - \frac{\Delta t}{2}(\widehat{w\mathbf{u}_z})_{ijk} \\ &\quad + \frac{\Delta t}{2}(\frac{1}{\mathbf{Re}}\nabla\cdot[\eta(\nabla\mathbf{u}^n_{ijk} + \nabla\mathbf{u}^{n\ T}_{ijk})] - \nabla p^{n-\frac{1}{2}}_{ijk} + F^n_{ijk}), \end{aligned} \tag{5.3.11}$$

$$\begin{aligned}\mathbf{u}^{n+\frac{1}{2},F}_{i,j+\frac{1}{2},k} &= \mathbf{u}^n_{i,j+1,k} - (\frac{\Delta y}{2} + \frac{v^n_{i,j+1,k}\Delta t}{2})\mathbf{u}^n_{y,i,j+1,k} - \frac{\Delta t}{2}(\widehat{u\mathbf{u}_x})_{i,j+1,k} - \frac{\Delta t}{2}(\widehat{w\mathbf{u}_z})_{i,j+1,k} \\ &\quad + \frac{\Delta t}{2}(\frac{1}{\mathbf{Re}}\nabla\cdot[\eta(\nabla\mathbf{u}^n_{i,j+1,k} + \nabla\mathbf{u}^{n\ T}_{i,j+1,k})] - \nabla p^{n-\frac{1}{2}}_{i,j+1,k} + F^n_{i,j+1,k}), \end{aligned} \tag{5.3.12}$$

$$\begin{aligned}\mathbf{u}^{n+\frac{1}{2},D}_{ij,k+\frac{1}{2}} &= \mathbf{u}^n_{ijk} + (\frac{\Delta z}{2} - \frac{w^n_{ijk}\Delta t}{2})\mathbf{u}^n_{z,ijk} - \frac{\Delta t}{2}(\widehat{u\mathbf{u}_x})_{ijk} - \frac{\Delta t}{2}(\widehat{v\mathbf{u}_y})_{ijk} \\ &\quad + \frac{\Delta t}{2}(\frac{1}{\mathbf{Re}}\nabla\cdot[\eta(\nabla\mathbf{u}^n_{ijk} + \nabla\mathbf{u}^{n\ T}_{ijk})] - \nabla p^{n-\frac{1}{2}}_{ijk} + F^n_{ijk}), \end{aligned} \tag{5.3.13}$$

$$\begin{aligned}\mathbf{u}^{n+\frac{1}{2},U}_{ij,k+\frac{1}{2}} &= \mathbf{u}^n_{ij,k+1} - (\frac{\Delta z}{2} + \frac{w^n_{ij,k+1}\Delta t}{2})\mathbf{u}^n_{z,i,j+1,k} - \frac{\Delta t}{2}(\widehat{u\mathbf{u}_x})_{ij,k+1} - \frac{\Delta t}{2}(\widehat{v\mathbf{u}_y})_{ij,k+1} \\ &\quad + \frac{\Delta t}{2}(\frac{1}{\mathbf{Re}}\nabla\cdot[\eta(\nabla\mathbf{u}^n_{ij,k+1} + \nabla\mathbf{u}^{n\ T}_{ij,k+1})] - \nabla p^{n-\frac{1}{2}}_{ij,k+1} + F^n_{ij,k+1}) \end{aligned} \tag{5.3.14}$$

Here, Δ^h is the standard seven -point finite difference approximation to the Laplacian. Above equations represent the final form of the predictor. Analogous formulae are used to predict values at each of the other edges of the cell. In evaluated using a monotonicity-limited fourth-order centered-difference slope approximation [8]. The limiting is done on the components of the velocity individually. The transverse derivative terms ($\widehat{v\mathbf{u}_y}$ in this case) are evaluated by first extrapolating from above and below to construct edge states, using normal derivatives only, and then choosing between these states using the upwinding procedure defined below. In particular, we define

$$
\begin{aligned}
\hat{\mathbf{u}}^L_{i+\frac{1}{2},jk} &= \mathbf{u}^n_{ijk} + (\frac{\Delta x}{2} - \frac{u_{ijk}\Delta t}{2})\mathbf{u}^n_{x,ijk} \\
\hat{\mathbf{u}}^R_{i+\frac{1}{2},jk} &= \mathbf{u}^n_{i+1,jk} - (\frac{\Delta x}{2} + \frac{u_{i+1,jk}\Delta t}{2})\mathbf{u}^n_{x,i+1,j} \\
\hat{\mathbf{u}}^B_{i,j+\frac{1}{2},k} &= \mathbf{u}^n_{ijk} + (\frac{\Delta y}{2} - \frac{v_{ijk}\Delta t}{2})\mathbf{u}^n_{y,ijk} \\
\hat{\mathbf{u}}^F_{i,j+\frac{1}{2},k} &= \mathbf{u}^n_{i,j+1,k} - (\frac{\Delta y}{2} + \frac{v_{i,j+1,k}\Delta t}{2})\mathbf{u}^n_{y,i,j+1,k} \\
\hat{\mathbf{u}}^D_{ij,k+\frac{1}{2}} &= \mathbf{u}^n_{ijk} + (\frac{\Delta z}{2} - \frac{w_{ijk}\Delta t}{2})\mathbf{u}^n_{z,ijk} \\
\hat{\mathbf{u}}^U_{ij,k+\frac{1}{2}} &= \mathbf{u}^n_{ij,k+1} - (\frac{\Delta z}{2} + \frac{w_{ij,k+1}\Delta t}{2})\mathbf{u}^n_{z,ij,k+1}
\end{aligned}
$$

where $\mathbf{u}_x, \mathbf{u}_y,$ and $\mathbf{u}_z$ are limited slopes in the x, y, and z-direction, respectively. Using the upwinding procedure we first define the normal advective velocity on the edges:

$$
\hat{u}^{adv}_{i+\frac{1}{2},jk} = \begin{cases} \hat{u}^L & \text{if } \hat{u}^L > 0, \quad \hat{u}^L + \hat{u}^R > 0, \\ \hat{u}^R & \text{if } \hat{u}^R < 0, \quad \hat{u}^L + \hat{u}^R < 0, \\ 0 & \text{otherwise.} \end{cases}
$$

$$
\hat{v}^{adv}_{i,j+\frac{1}{2},k} = \begin{cases} \hat{v}^B & \text{if } \hat{v}^B > 0, \quad \hat{v}^B + \hat{v}^F > 0, \\ \hat{v}^T & \text{if } \hat{v}^F < 0, \quad \hat{v}^B + \hat{v}^F < 0, \\ 0 & \text{otherwise.} \end{cases}
$$

$$
\hat{w}^{adv}_{ij,k+\frac{1}{2}} = \begin{cases} \hat{w}^D & \text{if } \hat{w}^D > 0, \quad \hat{w}^D + \hat{w}^U > 0, \\ \hat{w}^U & \text{if } \hat{w}^U < 0, \quad \hat{w}^D + \hat{w}^U < 0, \\ 0 & \text{otherwise.} \end{cases}
$$

(We suppress the $(i+\frac{1}{2}, j, k), \quad (i, j+\frac{1}{2}, k), \quad (ij, k+\frac{1}{2})$ spatial indices on the bottom and top states here and in the next equation.)

We now upwind **u** based on $\hat{u}^{adv}_{i+\frac{1}{2},jk}, \ \hat{v}^{adv}_{i,j+\frac{1}{2},k}, \ \hat{w}^{adv}_{ij,k+\frac{1}{2}}$:

$$
\hat{\mathbf{u}}_{i+\frac{1}{2},jk} = \begin{cases} \hat{\mathbf{u}}^L & \text{if } \hat{u}^{adv}_{i+\frac{1}{2},jk} > 0, \\ \frac{1}{2}(\hat{\mathbf{u}}^L + \hat{\mathbf{u}}^R) & \text{if } \hat{u}^{adv}_{i+\frac{1}{2},jk} = 0, \\ \hat{\mathbf{u}}^R & \text{if } \hat{u}^{adv}_{i+\frac{1}{2},jk} < 0. \end{cases}
$$

$$\hat{\mathbf{u}}_{i,j+\frac{1}{2},k} = \begin{cases} \hat{\mathbf{u}}^B & \text{if } \hat{v}^{adv}_{i,j+\frac{1}{2},k} > 0, \\ \frac{1}{2}(\hat{\mathbf{u}}^B + \hat{\mathbf{u}}^F) & \text{if } \hat{v}^{adv}_{i,j+\frac{1}{2},k} = 0, \\ \hat{\mathbf{u}}^F & \text{if } \hat{v}^{adv}_{i,j+\frac{1}{2},k} < 0. \end{cases}$$

$$\hat{\mathbf{u}}_{ij,k+\frac{1}{2}} = \begin{cases} \hat{\mathbf{u}}^D & \text{if } \hat{w}^{adv}_{ij,k+\frac{1}{2}} > 0, \\ \frac{1}{2}(\hat{\mathbf{u}}^D + \hat{\mathbf{u}}^U) & \text{if } \hat{w}^{adv}_{ij,k+\frac{1}{2}} = 0, \\ \hat{\mathbf{u}}^U & \text{if } \hat{w}^{adv}_{ij,k+\frac{1}{2}} < 0. \end{cases}$$

After constructing $\hat{\mathbf{u}}_{i-\frac{1}{2},jk}$, $\hat{\mathbf{u}}_{i,j-\frac{1}{2},k}$, $\hat{\mathbf{u}}_{ij,k-\frac{1}{2}}$ in a similar manner, we use these upwind values to form an approximation to the transverse derivative in (5.3.9 -5.3.14):

$$(\widehat{u\mathbf{u}_x})_{ijk} = \frac{1}{2\Delta x}(\hat{u}^{adv}_{i+\frac{1}{2},jk} + \hat{u}^{adv}_{i-\frac{1}{2},jk})(\hat{\mathbf{u}}_{i+\frac{1}{2},jk} - \hat{\mathbf{u}}_{i-\frac{1}{2},jk}).$$

$$(\widehat{v\mathbf{u}_y})_{ijk} = \frac{1}{2\Delta y}(\hat{v}^{adv}_{i,j+\frac{1}{2},k} + \hat{v}^{adv}_{i,j-\frac{1}{2},k})(\hat{\mathbf{u}}_{i,j+\frac{1}{2},k} - \hat{\mathbf{u}}_{i,j-\frac{1}{2},k}).$$

$$(\widehat{w\mathbf{u}_z})_{ijk} = \frac{1}{2\Delta z}(\hat{w}^{adv}_{ij,k+\frac{1}{2}} + \hat{w}^{adv}_{ij,k-\frac{1}{2}})(\hat{\mathbf{u}}_{ij,k+\frac{1}{2}} - \hat{\mathbf{u}}_{ij,k-\frac{1}{2}}).$$

Once we have computed $u^{n+\frac{1}{2},L/R}_{i+\frac{1}{2},jk}$, $v^{n+\frac{1}{2},B/F}_{i,j+\frac{1}{2},k}$, $v^{n+\frac{1}{2},D/U}_{ij,k+\frac{1}{2}}$, we are in a position to construct the normal face-centered edge velocities at $t^{n+\frac{1}{2}}$:

$$u^{ADV}_{i+\frac{1}{2},jk}, \;\; v^{ADV}_{i,j+\frac{1}{2},k}, \;\; w^{ADV}_{ij,k+\frac{1}{2}}.$$

Given $u^{n+\frac{1}{2},L/R}_{i+\frac{1}{2},jk}$, $v^{n+\frac{1}{2},B/F}_{i,j+\frac{1}{2},k}$, $v^{n+\frac{1}{2},D/U}_{ij,k+\frac{1}{2}}$,
we use an upwinding procedure to choose $u^{n+\frac{1}{2}}_{i+\frac{1}{2},jk}, v^{n+\frac{1}{2}}_{i,j+\frac{1}{2},k}$, and $w^{n+\frac{1}{2}}_{ij,k+\frac{1}{2}}$:

$$u^{n+\frac{1}{2}}_{i+\frac{1}{2},jk} = \begin{cases} u^L & \text{if } u^L > 0, \quad u^L + u^R > 0, \\ u^R & \text{if } u^R < 0, \quad u^L + u^R < 0, \\ 0 & \text{otherwise.} \end{cases}$$

$$v^{n+\frac{1}{2}}_{i,j+\frac{1}{2},k} = \begin{cases} v^B & \text{if } v^B > 0, \quad v^B + v^F > 0, \\ v^F & \text{if } v^F < 0, \quad v^B + v^F < 0, \\ 0 & \text{otherwise.} \end{cases}$$

$$w^{n+\frac{1}{2}}_{i,j+\frac{1}{2},k} = \begin{cases} w^D & \text{if } w^D > 0, \quad w^D + w^U > 0, \\ w^U & \text{if } w^U < 0, \quad w^D + w^U < 0, \\ 0 & \text{otherwise.} \end{cases}$$

These normal velocities on cell faces at $t^{n+\frac{1}{2}}$,

$$u^{n+\frac{1}{2}}_{i+\frac{1}{2},jk}, \quad v^{n+\frac{1}{2}}_{i,j+\frac{1}{2},k}, \quad w^{n+\frac{1}{2}}_{ij,k+\frac{1}{2}}$$

are second-order accurate but do not, in general, satisfy the discrete divergence-free condition. In order to make these velocities divergence-free, we apply the MAC projection [8].

The equation

$$D^{MAC} G^{MAC} \phi = D^{MAC} \mathbf{u}^{n+\frac{1}{2}}$$

is solved for ϕ, where

$$D^{MAC} \mathbf{u}^{n+\frac{1}{2}} = \frac{u^{n+\frac{1}{2}}_{i+\frac{1}{2},jk} - u^{n+\frac{1}{2}}_{i-\frac{1}{2},jk}}{\Delta x} + \frac{v^{n+\frac{1}{2}}_{i,j+\frac{1}{2},k} - v^{n+\frac{1}{2}}_{i,j-\frac{1}{2},k}}{\Delta y} + \frac{w^{n+\frac{1}{2}}_{ij,k+\frac{1}{2}} - v^{n+\frac{1}{2}}_{ij,k-\frac{1}{2}}}{\Delta z}$$

and

$$(G^{MAC}\phi)^x_{i+\frac{1}{2},jk} = \frac{\phi_{i+1,jk} - \phi_{ijk}}{\Delta x},$$
$$(G^{MAC}\phi)^y_{i,j+\frac{1}{2},k} = \frac{\phi_{i,j+1,k} - \phi_{ijk}}{\Delta y},$$
$$(G^{MAC}\phi)^z_{ij,k+\frac{1}{2}} = \frac{\phi_{ij,k+1} - \phi_{ijk}}{\Delta z}.$$

Then define advection velocities by

$$u^{ADV}_{i+\frac{1}{2},jk} := u^{n+\frac{1}{2}}_{i+\frac{1}{2},jk} - (G^{MAC}\phi)^x_{i+\frac{1}{2},jk},$$
$$v^{ADV}_{i,j+\frac{1}{2},k} := v^{n+\frac{1}{2}}_{i,j+\frac{1}{2},k} - (G^{MAC}\phi)^y_{i,j+\frac{1}{2},k},$$
$$w^{ADV}_{ij,k+\frac{1}{2}} := w^{n+\frac{1}{2}}_{ij,k+\frac{1}{2}} - (G^{MAC}\phi)^z_{ij,k+\frac{1}{2}}.$$

The next step, after constructing the advective velocities

$$u^{ADV}_{i+\frac{1}{2},jk}, \quad v^{ADV}_{i,j+\frac{1}{2},k}, \quad w^{ADV}_{ij,k+\frac{1}{2}}$$

is to choose the appropriate states $\mathbf{u}^{n+\frac{1}{2}}_{i+\frac{1}{2},jk}$, $\mathbf{c}^{n+\frac{1}{2}}_{i+\frac{1}{2},jk}$ given the left and right states:

$$\mathbf{u}^{n+\frac{1}{2},L/R}_{i+\frac{1}{2},jk}, \ \mathbf{c}^{n+\frac{1}{2},L/R}_{i+\frac{1}{2},jk}, \ \mathbf{u}^{n+\frac{1}{2},B/T}_{i,j+\frac{1}{2},k}, \ \mathbf{c}^{n+\frac{1}{2},B/F}_{i,j+\frac{1}{2},k}, \ \mathbf{u}^{n+\frac{1}{2},D/U}_{ij,k+\frac{1}{2}}, \ \mathbf{c}^{n+\frac{1}{2},D/U}_{ij,k+\frac{1}{2}}.$$

We have

$$\mathbf{u}^{n+\frac{1}{2}}_{i+\frac{1}{2},jk} = \begin{cases} \mathbf{u}^L & \text{if } u^{ADV} > 0, \\ \frac{1}{2}(\mathbf{u}^L + \mathbf{u}^R) & \text{if } u^{ADV} = 0, \\ \mathbf{u}^R & \text{if } u^{ADV} < 0, \end{cases}$$

$$\mathbf{u}^{n+\frac{1}{2}}_{i,j+\frac{1}{2},k} = \begin{cases} \mathbf{u}^B & \text{if } v^{ADV} > 0, \\ \frac{1}{2}(\mathbf{u}^B + \mathbf{u}^F) & \text{if } v^{ADV} = 0, \\ \mathbf{u}^F & \text{if } v^{ADV} < 0, \end{cases}$$

$$\mathbf{u}^{n+\frac{1}{2}}_{ij,k+\frac{1}{2}} = \begin{cases} \mathbf{u}^D & \text{if } w^{ADV} > 0, \\ \frac{1}{2}(\mathbf{u}^D + \mathbf{u}^U) & \text{if } w^{ADV} = 0, \\ \mathbf{u}^U & \text{if } w^{ADV} < 0, \end{cases}$$

$$c^{n+\frac{1}{2}}_{i+\frac{1}{2},jk} = \begin{cases} c^L & \text{if } u^{ADV} > 0, \\ \frac{1}{2}(c^L + c^R) & \text{if } u^{ADV} = 0, \\ c^R & \text{if } u^{ADV} < 0, \end{cases}$$

$$c^{n+\frac{1}{2}}_{i,j+\frac{1}{2},k} = \begin{cases} c^B & \text{if } v^{ADV} > 0, \\ \frac{1}{2}(c^B + c^F) & \text{if } v^{ADV} = 0, \\ c^F & \text{if } v^{ADV} < 0, \end{cases}$$

$$c^{n+\frac{1}{2}}_{ij,k+\frac{1}{2}} = \begin{cases} c^D & \text{if } w^{ADV} > 0, \\ \frac{1}{2}(c^D + c^U) & \text{if } w^{ADV} = 0, \\ c^U & \text{if } w^{ADV} < 0, \end{cases}$$

where we have again suppressed the spatial indices $(i+\frac{1}{2},jk),\ (i,j+\frac{1}{2},k)$ and $(i,j,k+\frac{1}{2})$. We follow a similar procedure to construct $\mathbf{u}_{i-\frac{1}{2},jk},\ \mathbf{u}_{i,j-\frac{1}{2},k}$ and $\mathbf{u}_{ij,k-\frac{1}{2}}$.

$$\begin{aligned}[\mathbf{u}\cdot\nabla\mathbf{u}]^{n+\frac{1}{2}} = u\mathbf{u}_x + v\mathbf{u}_y + w\mathbf{u}_z &= \frac{1}{2\Delta x}(u^{ADV}_{i+\frac{1}{2},jk} + u^{ADV}_{i-\frac{1}{2},jk})(\mathbf{u}_{i+\frac{1}{2},jk} - \mathbf{u}_{i-\frac{1}{2},jk}) \\ &+ \frac{1}{2\Delta y}(v^{ADV}_{i,j+\frac{1}{2},k} + v^{ADV}_{i,j-\frac{1}{2},k})(\mathbf{u}_{i,j+\frac{1}{2},k} - \mathbf{u}_{i,j-\frac{1}{2},k}) \\ &+ \frac{1}{2\Delta z}(w^{ADV}_{ij,k+\frac{1}{2}} + w^{ADV}_{ij,k-\frac{1}{2}})(\mathbf{u}_{ij,k+\frac{1}{2}} - \mathbf{u}_{ij,k-\frac{1}{2}}).\end{aligned}$$

$$\begin{aligned}[\mathbf{u}\cdot\nabla c]^{n+\frac{1}{2}} = uc_x + vc_y + wc_z &= \frac{1}{2\Delta x}(u^{ADV}_{i+\frac{1}{2},jk} + u^{ADV}_{i-\frac{1}{2},jk})(c_{i+\frac{1}{2},jk} - c_{i-\frac{1}{2},jk}) \\ &+ \frac{1}{2\Delta y}(v^{ADV}_{i,j+\frac{1}{2},k} + v^{ADV}_{i,j-\frac{1}{2},k})(c_{i,j+\frac{1}{2},k} - c_{i,j-\frac{1}{2},k}) \\ &+ \frac{1}{2\Delta z}(w^{ADV}_{ij,k+\frac{1}{2}} + v^{ADV}_{ij,k-\frac{1}{2}})(c_{ij,k+\frac{1}{2}} - c_{ij,k-\frac{1}{2}}).\end{aligned}$$

The Godunov method is an explicit difference scheme and, as such, requires a time-step restriction. A linear, constant-coefficient analysis shows that for stability we must require

$$\max_{ijk}\left(\frac{|u_{ijk}|\Delta t}{\Delta x}, \frac{|v_{ijk}|\Delta t}{\Delta y}, \frac{|w_{ijk}|\Delta t}{\Delta z}\right) = \sigma \leq 1,$$

where σ is the CFL number. The time-step restriction of the Godunov method is used to set the time step for the overall algorithm.

3.A Discretization of the projection

In this section we describe the "approximate projection" in Step 2.

Given the discrete vector field

$$\frac{\mathbf{u}^* - \mathbf{u}^n}{\Delta t}, \tag{5.3.15}$$

we decompose (5.3.15) into *approximately* divergence free part

$$\frac{\mathbf{u}^{n+1} - \mathbf{u}^n}{\Delta t} \tag{5.3.16}$$

and the discrete gradient of a scalar ϕ, i.e.,

$$\frac{\mathbf{u}^* - \mathbf{u}^n}{\Delta t} = \frac{\mathbf{u}^{n+1} - \mathbf{u}^n}{\Delta t} + \nabla\phi, \tag{5.3.17}$$

where the discrete gradient ∇ in (5.3.17) is defined as

$$
\begin{aligned}
\nabla\phi_{ijk} \quad = \quad & \Bigg(\frac{\phi_{i+\frac{1}{2},j+\frac{1}{2},k+\frac{1}{2}} + \phi_{i+\frac{1}{2},j-\frac{1}{2},k+\frac{1}{2}} + \phi_{i+\frac{1}{2},j+\frac{1}{2},k-\frac{1}{2}} + \phi_{i+\frac{1}{2},j-\frac{1}{2},k-\frac{1}{2}}}{4\Delta x} \\
& - \frac{\phi_{i-\frac{1}{2},j+\frac{1}{2},k+\frac{1}{2}} + \phi_{i-\frac{1}{2},j-\frac{1}{2},k+\frac{1}{2}} + \phi_{i-\frac{1}{2},j+\frac{1}{2},k-\frac{1}{2}} + \phi_{i-\frac{1}{2},j-\frac{1}{2},k-\frac{1}{2}}}{4\Delta x}, \\
& \frac{\phi_{i+\frac{1}{2},j+\frac{1}{2},k+\frac{1}{2}} + \phi_{i-\frac{1}{2},j+\frac{1}{2},k+\frac{1}{2}} + \phi_{i+\frac{1}{2},j+\frac{1}{2},k-\frac{1}{2}} + \phi_{i-\frac{1}{2},j+\frac{1}{2},k-\frac{1}{2}}}{4\Delta y} \\
& - \frac{\phi_{i+\frac{1}{2},j-\frac{1}{2},k+\frac{1}{2}} + \phi_{i-\frac{1}{2},j-\frac{1}{2},k+\frac{1}{2}} + \phi_{i+\frac{1}{2},j-\frac{1}{2},k-\frac{1}{2}} + \phi_{i-\frac{1}{2},j-\frac{1}{2},k-\frac{1}{2}}}{4\Delta y}, \\
& \frac{\phi_{i+\frac{1}{2},j+\frac{1}{2},k+\frac{1}{2}} + \phi_{i-\frac{1}{2},j+\frac{1}{2},k+\frac{1}{2}} + \phi_{i+\frac{1}{2},j-\frac{1}{2},k+\frac{1}{2}} + \phi_{i-\frac{1}{2},j-\frac{1}{2},k+\frac{1}{2}}}{4\Delta z} \\
& - \frac{\phi_{i+\frac{1}{2},j+\frac{1}{2},k-\frac{1}{2}} + \phi_{i-\frac{1}{2},j+\frac{1}{2},k-\frac{1}{2}} + \phi_{i+\frac{1}{2},j-\frac{1}{2},k-\frac{1}{2}} + \phi_{i-\frac{1}{2},j-\frac{1}{2},k-\frac{1}{2}}}{4\Delta z} \Bigg).
\end{aligned}
$$

The approximate projection is computed by solving

$$
\Delta\phi = \nabla \cdot \left(\frac{\mathbf{u}^* - \mathbf{u}^n}{\Delta t} \right) \tag{5.3.18}
$$

for ϕ, where

$$
\Delta\phi_{ijk} \quad = \quad \frac{\phi_{i+1,jk} - 2\phi_{ijk} + \phi_{i-1,jk}}{\Delta x^2} + \frac{\phi_{i,j+1,k} - 2\phi_{ijk} + \phi_{i,j-1,k}}{\Delta y^2} + \frac{\phi_{ij,k+1} - 2\phi_{ijk} + \phi_{ij,k-1}}{\Delta z^2}.
$$

and

$$
\begin{aligned}
\nabla \cdot \mathbf{u}_{i+\frac{1}{2},j+\frac{1}{2},k+\frac{1}{2}} \quad = \quad & \frac{u_{i+1,j+1,k+1} + u_{i+1,j-1,k+1} + u_{i+1,j+1,k-1} + u_{i+1,j-1,k-1}}{4\Delta x} \\
& - \frac{u_{i-1,j+1,k+1} + u_{i-1,j-1,k+1} + u_{i-1,j+1,k-1} + u_{i-1,j-1,k-1}}{4\Delta x} \\
& + \frac{v_{i+1,j+1,k+1} + v_{i-1,j+1,k+1} + v_{i+1,j+1,k-1} + v_{i-1,j+1,k-1}}{4\Delta y} \\
& - \frac{v_{i+1,j-1,k+1} + v_{i-1,j-1,k+1} + v_{i+1,j-1,k-1} + v_{i-1,j-1,k-1}}{4\Delta y} \\
& + \frac{w_{i+1,j+1,k+1} + w_{i-1,j+1,k+1} + w_{i+1,j-1,k+1} + w_{i-1,j-1,k+1}}{4\Delta z} \\
& - \frac{w_{i+1,j+1,k-1} + w_{i-1,j+1,k-1} + w_{i+1,j-1,k-1} + w_{i-1,j-1,k-1}}{4\Delta z}.
\end{aligned}
$$

After (5.3.18) is solved, we get $\mathbf{u}^{n+1}$,

$$
\mathbf{u}^{n+1} = \mathbf{u}^* - \Delta t \nabla\phi,
$$

and update $p^{n+\frac{1}{2}}$,

$$
p^{n+\frac{1}{2}} = p^{n-\frac{1}{2}} + \phi.
$$

5.4 Cocontinuity detection algorithm

We define a measure of cocontinuity as follows. We first determine n the number of connected components of the flow. Then, for each component that touches all six boundaries of the box, we define the degree of cocontinuity of that phase: $d_i = V_i/V$ where V_i is the volume of the phase and V is the total volume of the dispersed phase. The structure is fully cocontinuous $n = 1$ and $V_i/V = 1$. A blend is only considered fully cocontinuous if 100 % of one of the components can be extracted and the remaining piece is still self-supporting.

To find the degree of cocontinuity in our numerical simulation, we developed the following cocontinuity detection algorithm. The algorithm starts with the point, (1,1,1) in the cubic domain, $nx \times ny \times nz$. For a given cubic array $A[\,][\,][\,]$, we want to find how many connected components it has and the degree of cocontinuity of each component.

Begin algorithm

components $= 0$;

cocontinuity $= 0.0$;

total = $\sum_{A[i][j][k]>0.5} 1$,

$for\ (k = 1;\ k <= nz;\ k++)\{$

$for\ (j = 1;\ j <= ny;\ j++)\{$

$for\ (i = 1;\ i <= nx;\ i++)\{$

$if\ (A[i][j][k] > 0.5)\{$

$m = i,\ \ n = j,\ \ l = k;$

$flag1 = 0,\ \ flag2 = 1,\ \ count = 1;$

$$for\ (ii = 1;\ ii <= nx;\ ii++)\{$$
$$for\ (jj = 1;\ jj <= ny;\ jj++)\{$$
$$for\ (kk = 1;\ kk <= nz;\ kk++)\{$$
$$B[ii][jj][kk] = 0.0;$$
$$\}$$
$$\}$$
$$\}$$

```
while (flag1 < flag2) {
    detection(A, B, m, n, l, register);
    flag1++;
        m = register[i][1];
        n  = register[i][2];
        l   = register[i][3];
    flag2 = count;
}

component++;
```

Check whether B[ ][ ][ ] touches all six boundaries, then this component is continuous and cocontinuity of this connection component is $(\sum_{B[i][j][k]>0.5} 1)$ /total, otherwise it is not cocontinuous.

```
void detection(double ***A, double ***B, int m, int n, int l, int register[][4])
{
        B[m][n][l] = 1.0;
        A[m][n][l] = 0.0;

    for (i=-1; i ≤1; i=i+1) {
        for (j=-1; j≤ 1; j=j+1) {
            for (k=-1; k ≤ 1; k=k+1) {

    if ( 0 < m + i < nx + 1 and 0 < n + j < ny + 1 and 0 < l + k < nz + 1 ) {
```

```
if (A[i+m][j+n][k+l] > 0.5) {

count=count+1;
    register[count-1][1] = i+m;
    register[count-1][2] = j+n;
    register[count-1][3] = k+l;

    B[i+m][j+n][k+l] = A[i+m][j+n][k+l];
    A[i+m][j+n][k+l] = 0.0;   }
                    }
                }
            }
        }
    }
End algorithm
```

5.5 Numerical Simulations

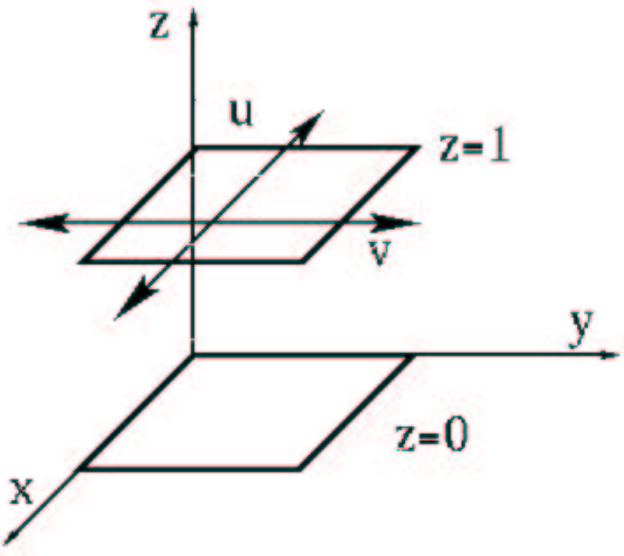

Figure 5.6: Schematic of computational domain

Simulations are for Newtonian viscous fluids. The domain is [0,1]x[0,1]x[0,1] with periodic boundary conditions applied on the side walls and the chaotic shear is applied at the $z = 0, 1$ walls 5.6. That is

$$u(x, y, 1) = -u(x, y, 0) = \sin(\pi t/T),$$
$$v(x, y, 1) = -v(x, y, 0) = \cos(\pi t/T),$$

where t is the time and T is a period. See the reference [102] for the details about the chaotic shear boundary conditions. The flow is started from rest and the initial concentration field consists of either randomly distributed ellipsoids at specific volume fractions (Figs. 5.7-5.27) or random perturbations of the uniform concentration consistent with the specified volume fraction (Figs. 5.33-5.36).

The simulation parameters are

$$\eta_1/\eta_2 = 1.0, \;\; \rho_1/\rho_2 = 1.0, \;\; \mathbf{Re} = 1.0, \;\; \mathbf{We} = 100.0; \;\; \epsilon = 0.01, \;\; \mathbf{Pe} = 10.0/\epsilon,$$

these nondimensional parameters were defined at chapter 4. At high enough volume fractions (35% or greater), the initial distribution undergoes a coalescence cascade and co-continuous microstructures form, consistent with experimental observations [66].

Fig. 5.7 shows 20 % volume fraction interface and Fig. 5.8, Fig. 5.9, and Fig. 5.10 are 2-D slices of the concentration field normal to x-axis, y-axis, and z-axis, respectively. In these plots, the $c = 0.5$ contours are shown as filled. Similarly, Figs. 5.11, 5.15, 5.15, 5.15, 5.19, 5.23, and 5.27 show 25 %, 30 %, 35 %, 40 %, 45 %, and 50 % volume fractions. In these figures, the interfacial surface corresponding to $c = 0.5$ is plotted. Convex particles, such as a disk suspended in a matrix, have a convex area equal to the real area and thus have zero surrounded area. Particles that have some concave interface structure will 'surround' the material in the concave area. In systems where the two phases are heavily inter-wined, each phase surrounds a significant amount of the other phase. This idea is exploited in the 2-D image analysis in [72] that is used to detect co-continuous structures. In the 2-D slices we have shown here, this effect can be seen although much more information is gained by viewing and analyzing the full 3D domain.

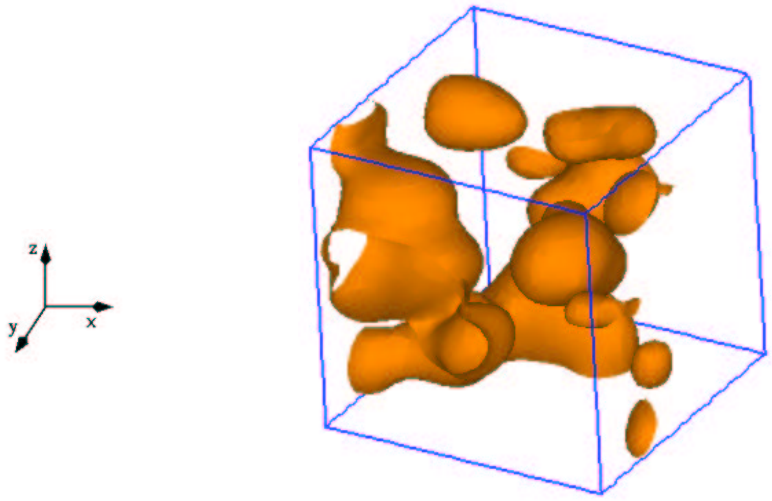

Figure 5.7: 20 % volume fraction

Figure 5.8: x slices (x=0.2, 0.3 and 0.8)

Figure 5.9: y slices (y=0.2, 0.3 and 0.8)

Figure 5.10: z slices (z=0.2, 0.3 and 0.8)

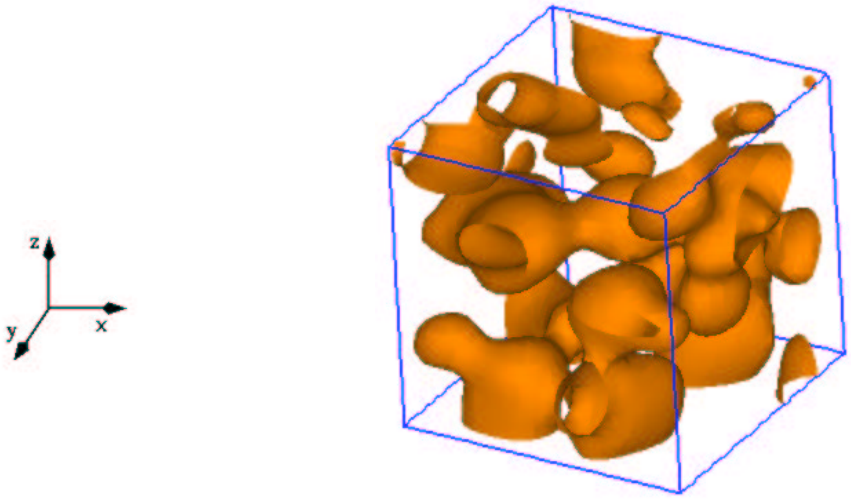

Figure 5.11: 30 % volume fraction

Figure 5.12: x slices (x=0.2, 0.3 and 0.8)

Figure 5.13: y slices (y=0.2, 0.3 and 0.8)

Figure 5.14: z slices (z=0.2, 0.3 and 0.8)

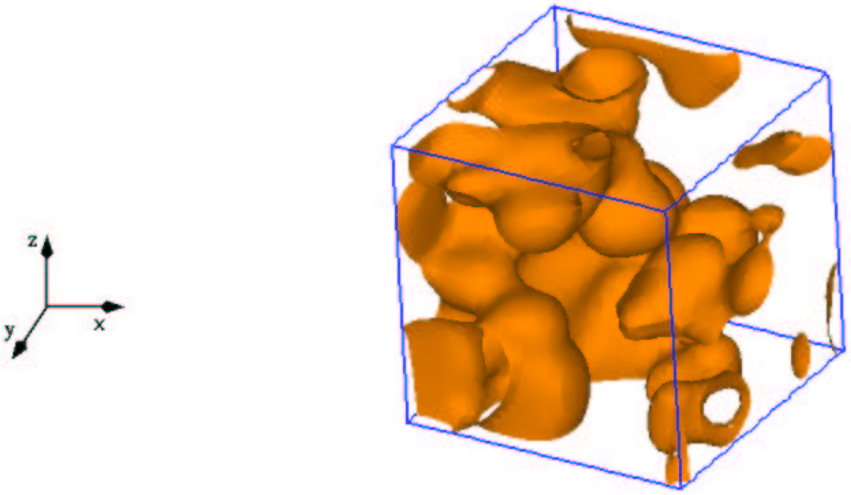

Figure 5.15: 35 % volume fraction

Figure 5.16: x slices (x=0.2, 0.3 and 0.8)

Figure 5.17: y slices (y=0.2, 0.3 and 0.8)

Figure 5.18: z slices (z=0.2, 0.3 and 0.8)

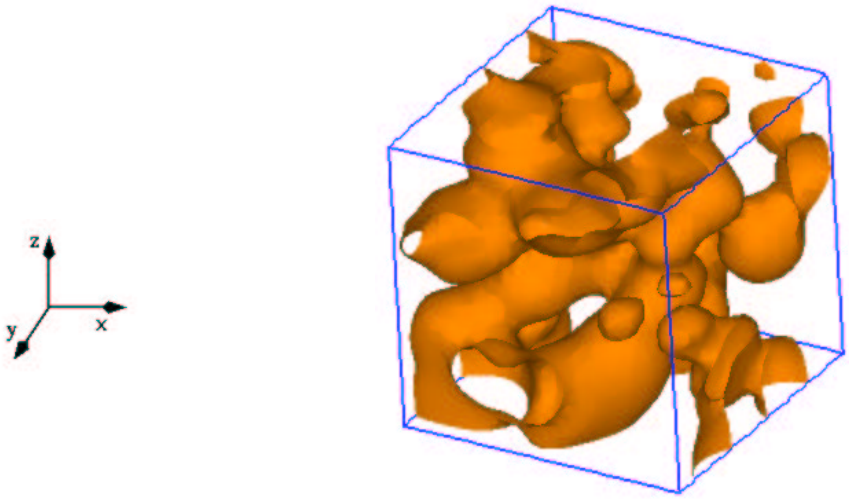

Figure 5.19: 40 % volume fraction

Figure 5.20: x slices (x=0.2, 0.3 and 0.8)

Figure 5.21: y slices (y=0.2, 0.3 and 0.8)

Figure 5.22: z slices (z=0.2, 0.3 and 0.8)

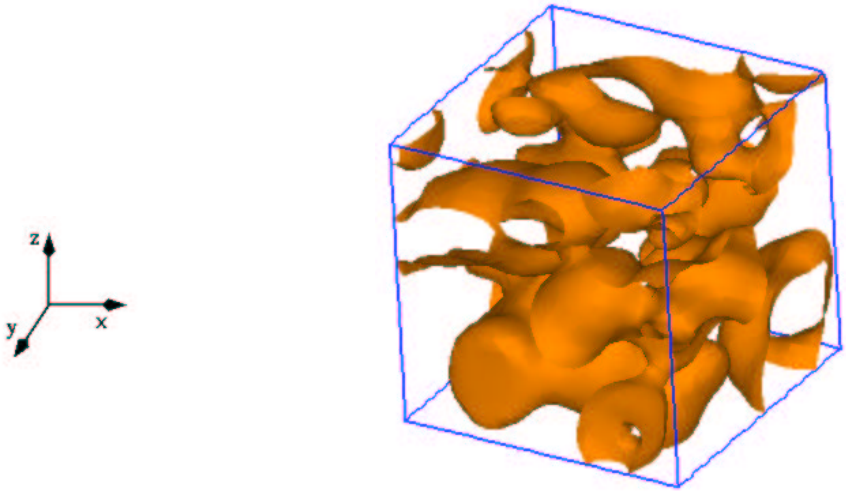

Figure 5.23: 45 % volume fraction

Figure 5.24: x slices (x=0.2, 0.3 and 0.8)

Figure 5.25: y slices (y=0.2, 0.3 and 0.8)

Figure 5.26: z slices (z=0.2, 0.3 and 0.8)

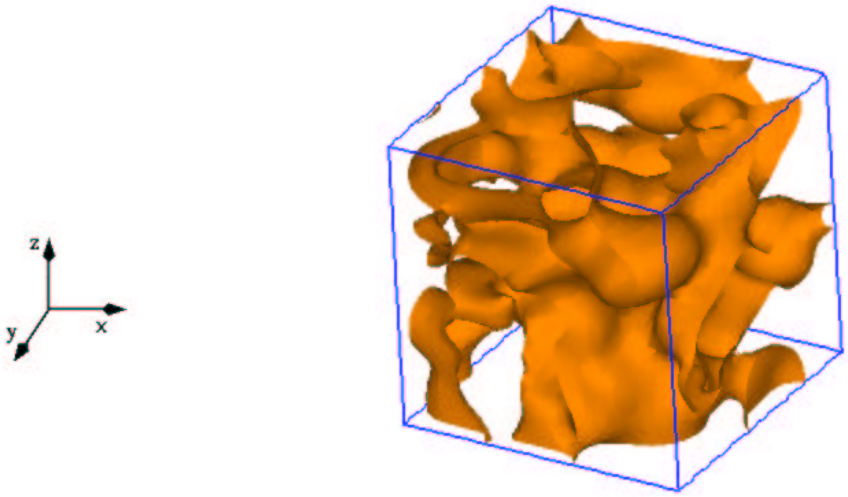

Figure 5.27: 50 % volume fraction

Figure 5.28: x slices (x=0.2, 0.3 and 0.8)

Figure 5.29: y slices (y=0.2, 0.3 and 0.8)

Figure 5.30: z slices (z=0.2, 0.3 and 0.8)

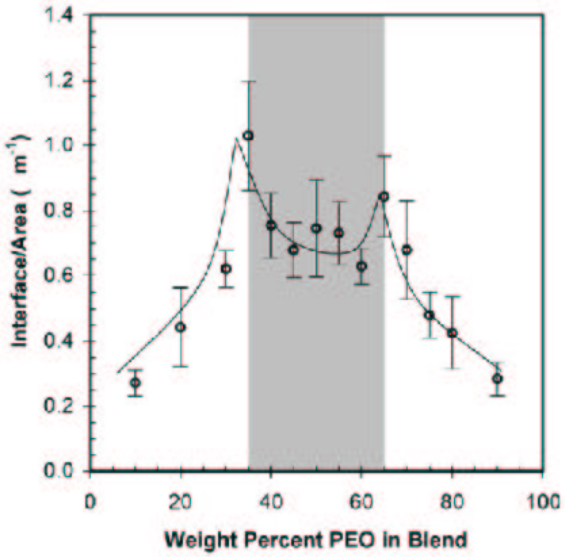

Figure 5.31: Experiment result [66].

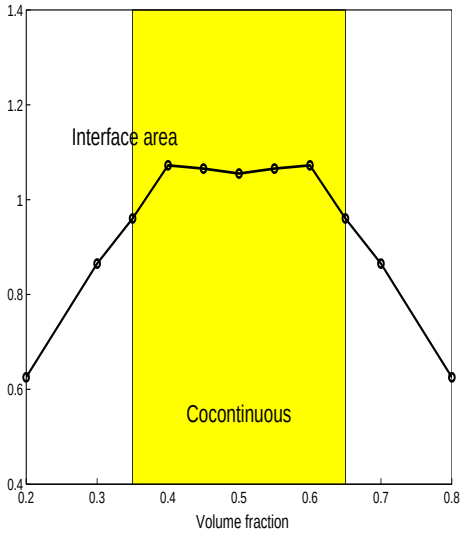

Figure 5.32: Numerical simulation

5.A Interfacial area per unit area

Experimentally [66], the interfacial area per unit volume exhibits a maxima for blend compositions at the boundary between droplet and cocontinuous morphologies. This is seen in Fig. 5.31, the average length of interface per unit area of the micrographs is shown as a function of blend composition. Two local maxima appear in this plot, one at a blend composition of 35% PEO and another at a composition of 65% PEO. Solvent extraction experiments confirmed that these peaks represent the boundaries of the region of cocontinuity for these PEO-PS polymer blends [67]. Blends outside of this region have droplet morphologies, while blends within this region exhibit cocontinuous microstructures. This suggests that, like solvent extraction, interfacial area measurement using SEM with image analysis can be used to detect the region of cocontinuity in a polymer-polymer system. In Fig. 5.32, the corresponding numerical results (interface area per unit area) are shown with different volume fractions. Unlike the experiments, peaks in the area curve are observed at 40% and 60% volume fractions. Consistent with the experiments, the interface area is roughly flat within the co-continuous domain. There are several possible explanations for this deviation that are currently under study. For example, in the experiment, there is significant annealing of the blend before the area measurement is taken (Macosko, private communication). Moreover, the experimental fluids are non-Newtonian and viscoelastic effects are neglected in our simulations.

In Figs. 5.33-5.36, the evolution of an initially fine, random dispersion of drops (30%, 35%, 45%,

and 50% volume fractions) under simple shear (shear rate $\dot{\gamma} = 1.0$) are shown. Observe the development of structure. To characterize the structure, we define a measure of cocontinuity as follows. We first determine n the number of connected components of the flow. Then, for each component that touches all six boundaries of the box, we define the degree of cocontinuity of that phase: $d_i = V_i/V$ where V_i is the volume of the phase and V is the total volume of the dispersed phase. The structure is fully cocontinuous $n = 1$ and $V_i/V = 1$.

Interpretation of the cocontinuity function

Values of the cocontinuity that are near zero indicate discrete, convex particles suspended in a matrix. As the cocontinuity approaches 0.3, some combination of increased suspended phase and partially concave discrete particle morphology is present in the image. Cocontinuity values from 0.3 to 0.6 are obtained when the particle-matrix interface morphology is significantly concave without much interpenetration of the particles from the same phases or, in special cases of highly coordinated structures, from the same phase.

The degree of cocontinuity d_i for this flow is presented in the tables below each simulation result. In all cases, we find that there is never more than a single component in contact with all the boundaries. For example, when the volume fraction is 35%, a cocontinuous structure forms approximately at time $t = 1.95$ and persists until approximately $t = 6.75$. The structure is formed by a coalescence cascade and is eventually broken by the simple shearing flow. The final flow configuration consists of a series of fiber-like tubes of second-phase fluid.

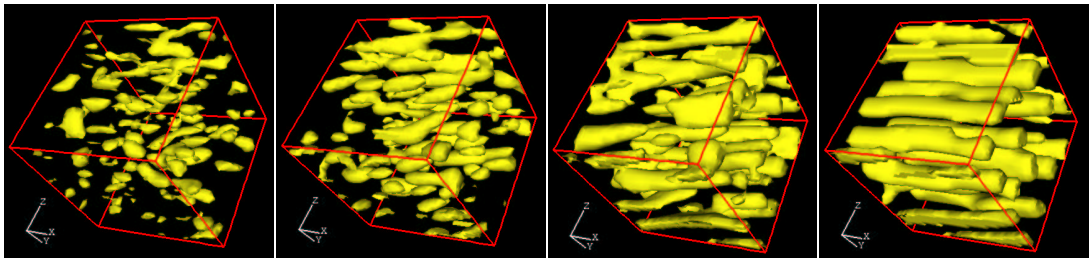

t=0.3 t=1.35 t=4.2 t=10.05

Figure 5.33: 30 % volume fraction

case 30 %	t=0.3	1.35	1.8	1.95	4.2	6.9	10.05
connected components	154	85	68	68	29	23	20
cocontinuity	0.0	0.0	0.0	0.0	0.0	0.0	0.0

Table 5.1: Cocontinuity of 30 % concentration of dispersed phase

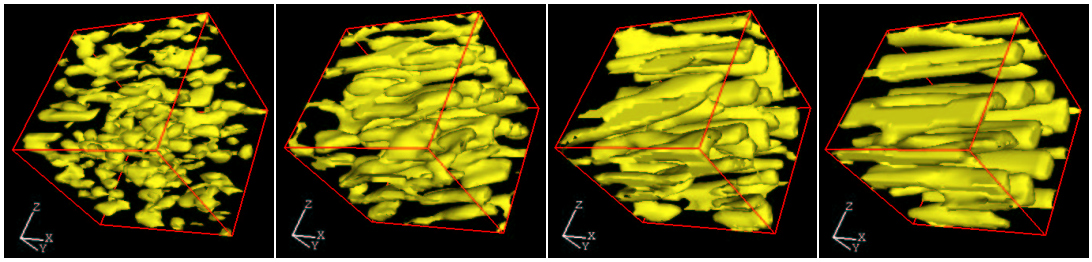

t=0.3 t=1.35 t=4.2 t=10.05

Figure 5.34: 35 % volume fraction

case 35 %	t=0.3	1.35	1.8	1.95	4.2	6.9	10.05
connected components	126	44	30	26	10	13	15
cocontinuity	0.0	0.0	0.0	0.0	0.95	0.0	0.0

Table 5.2: Cocontinuity of 35% concentration of dispersed phase

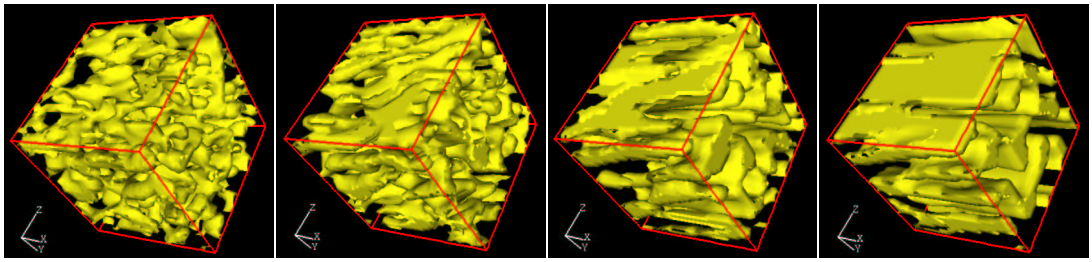

t=0.3 t=1.35 t=4.2 t=10.05

Figure 5.35: 45% volume fraction

case 45 %	t=0.3	1.35	1.8	1.95	4.2	6.9	10.05
connected components	11	4	4	1	1	2	5
cocontinuity	0.996	0.999	0.998	1.0	1.0	0.998	0.935

Table 5.3: Cocontinuity of 45% concentration of dispersed phase

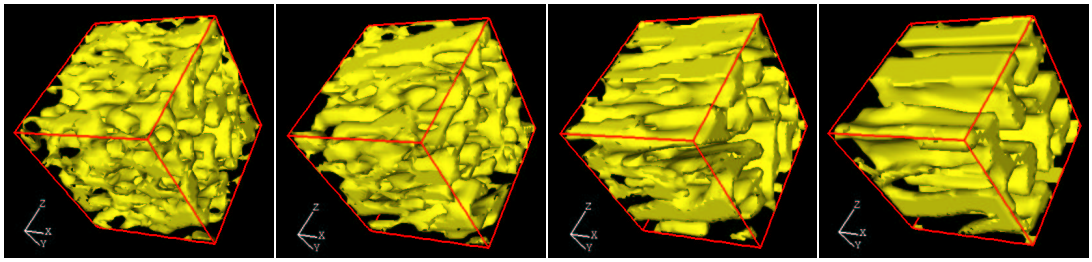

t=0.3 t=1.35 t=4.2 t=10.05

Figure 5.36: 50% volume fraction

case 50 %	t=0.3	1.35	1.8	1.95	4.2	6.9	10.05
connected components	4	6	2	1	2	3	3
cocontinuity	0.999	0.999	0.9999	1.0	0.9999	0.999	0.0

Table 5.4: Cocontinuity of 50% concentration of dispersed phase

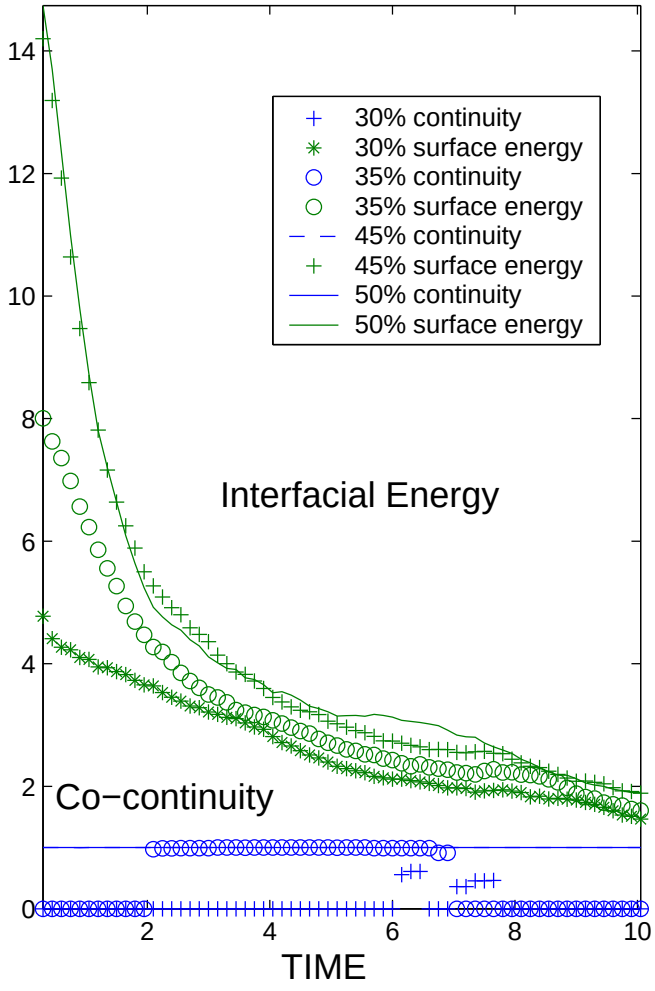

Figure 5.37: The values of cocontinuity and interface Energy are plotted against time

Finally, in Fig. 5.37 the total interface area per unit area and the degree of cocontinuity are plotted as functions of time for the simulations presented in Figs. 5.33-5.36 . All volume fractions show a decrease in interface area. The 30% case shows zero cocontinuity until time $t = 6.0$, and has a degree of cocontinuity approximately 0.5 in the time interval $t = 6.0$ and $t = 8.0$. The 35% is co-continuous between $t = 2.0$ and $t = 7.0$. The 45% and 50% are cocontinuous throughout the simulation. This is due in part to the choice of initial conditions and is currently under study.

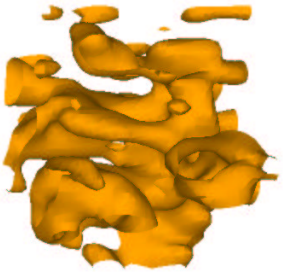

Figure 5.38: t=0

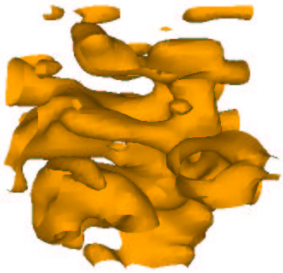

Figure 5.39: t=0

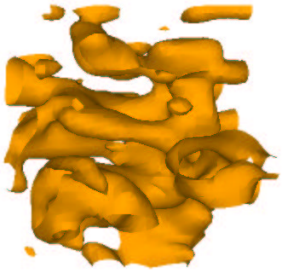

Figure 5.40: t=1500

Figure 5.41: t=1500

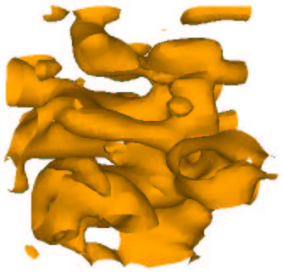

Figure 5.42: t=3500

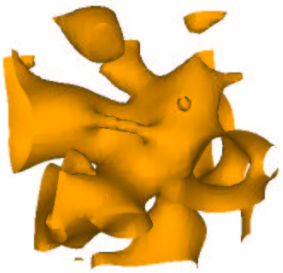

Figure 5.43: t=3500

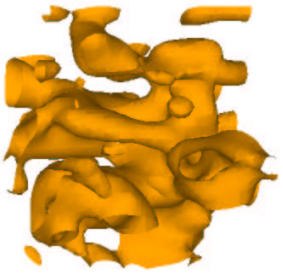

Figure 5.44: t=5000

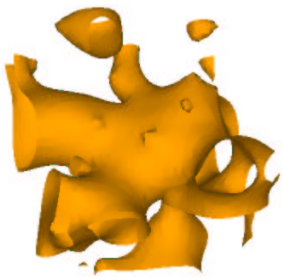

Figure 5.45: t=5000

Figure 5.46: Left column $\sigma = 1.0$, right column $\sigma = 50.0$

5.B The Influence of interfacial tension

In Fig. 5.46, evolutions are presented using two different surface tensions. The first column in the figure is the evolution with $\sigma = 1.0$, and the second is with $\sigma = 50.0$. And the initial configurations are same and the other parameters are as in Fig. (5.7) except that there is no applied shear flow. The evolution is driven by surface tension relaxation. In the $\sigma = 1$ case, there is little observed evolution. In the $\sigma = 50$ case, on the other hand, there is much more rapid evolution and there is break-up due to the Rayleigh instability and a subsequent coarsening of microstructure through interface coalescence.

5.C Conclusions

Numerical simulations show qualitative agreement with experimental data. Surface tension, flow field, and volume fractions are all important factors for the blends to form cocontinuous morphologies.